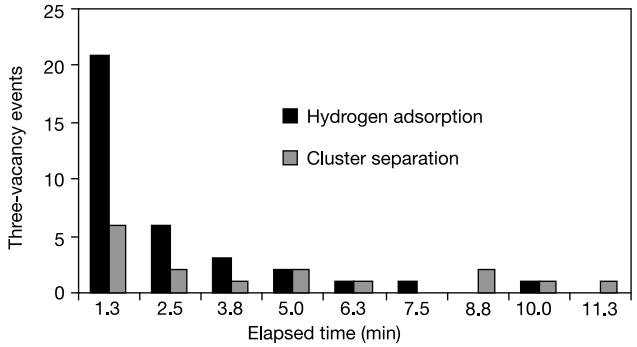


**Figure 4** Lifetimes of three-vacancy clusters. Shown is the observed lifetime distribution of three-vacancy (3V) clusters at 65 K in a background pressure of $\sim 2 \times 10^{-7}$ torr $H_2$. The clusters decay either by separation or by annihilation following adsorption of a $H_2$ molecule, which fills two of the three H vacancies.

atoms diffusing rapidly among the six sites. In contrast to the 2V clusters, the larger 3V clusters are active for $H_2$ dissociation (Fig. 2c). The 2V cluster has separated into isolated vacancies (A, B), while the 3V cluster has been annihilated by a dissociating $H_2$ molecule, leaving one vacancy (C) behind. Two other 2V clusters have remained intact during this process, but separate several frames later (not shown). The annihilation of 3V clusters occurs only in the presence of $H_2$ background gas.

As a final example, Fig. 3 shows the formation and annihilation of a 4V cluster. Again, this cluster appears as a triangle bounded by {110} edges and occupying an area containing ten Pd atoms. The six H atoms in the triangle diffuse rapidly among the ten sites. This cluster decayed via $H_2$ adsorption, leaving a pair of isolated vacancies. For this and for larger vacancy clusters, annihilation by $H_2$ adsorption was the dominant decay mechanism.

Figure 4 shows the observed lifetime distribution for 3V clusters in $2 \times 10^{-7}$ torr of $H_2$, and Table 1 gives statistics for 2V to 5V clusters. Hydrogen adsorption was frequently observed for 3V and larger clusters, always reducing the number of vacancies by two. The $H_2$ sticking probability can be estimated at 0.5–0.8% for 3V and larger clusters. In contrast, we never observed $H_2$ adsorption for a 2V cluster even though two atomic hydrogen sites are available. This finding is contrary to accepted models of diatomic molecule dissociation, and calls for a theoretical effort in modelling the adsorption step in catalysis that includes the precise atomic structure of the target sites and the role of adsorbate diffusivity in generating such sites.

As a first step to understanding the dynamics of vacancy aggregation, we performed Monte Carlo simulations of vacancy diffusion. The model, which uses only experimentally estimated values of the diffusion barriers of H atoms and vacancies (ref. 11; see also http://stm.lbl.gov), correctly reproduced the observed stability and the triangular appearance of the 2V, 3V and 4V clusters, and could thus help to improve our molecular-level understanding of the formation of the active sites that determine the activity of catalytically active surfaces. □

Received 13 January; accepted 4 March 2003; doi:10.1038/nature01557.

1. Conrad, H., Ertl, G. & Latta, E. E. Adsorption of hydrogen on palladium single crystal surfaces. *Surf. Sci.* **41,** 435–446 (1974).
2. Taylor, H. S. Theory of the catalytic surface. *Proc. R. Soc. Lond. A* **108,** 105–111 (1925).
3. Boudart, M. Four decades of active centers. *Am. Sci.* **57,** 97–111 (1969).
4. Ponec, V. & Sachtler, W. M. H. The reactions between cyclopentane and deuterium on nickel and nickel-copper alloys. *J. Catal.* **24,** 250–261 (1972).
5. Sinfelt, J. H. *Bimetallic Catalysts: Discoveries, Concepts and Applications* (Wiley and Sons, New York, 1983).
6. Somorjai, G. A. *Introduction to Surface Chemistry and Catalysis* (Wiley and Sons, New York, 1994).
7. Behler, S. *et al.* A scanning tunneling microscope with continuous flow cryostat sample cooling. *Rev. Sci. Instrum.* **68,** 2479–2485 (1997).
8. Felter, T. E., Sowa, E. C. & Van Hove, M. A. Location of hydrogen on palladium (111) studied by low-energy electron diffraction. *Phys. Rev. B* **40,** 891–899 (1989).
9. Paul, J. F. & Sautet, P. Density-functional periodic study of the adsorption of hydrogen on a palladium (111) surface. *Phys. Rev. B* **53,** 8015–8027 (1996).
10. Lovvik, O. M. & Olsen, R. A. Adsorption energies and ordered structures of hydrogen on Pd(111) from density functional periodic calculations. *Phys. Rev. B* **58,** 10890–10898 (1998).
11. Mitsui, T., Rose, M. K., Fomin, E., Ogletree, D. F. & Salmeron, M. Hydrogen adsorption and diffusion on Pd(111). *Surf. Sci.* (submitted).

**Supplementary Information** accompanies the paper on *Nature*'s website (http://www.nature.com/nature).

**Acknowledgements** This work was supported by the Office of Basic Energy Science of the US Department of Energy.

**Competing interests statement** The authors declare that they have no competing financial interests.

**Correspondence** and requests for materials should be addressed to M.S. (e-mail: salmeron@stm.lbl.gov).

# Global anisotropy and the thickness of continents

**Yuancheng Gung, Mark Panning & Barbara Romanowicz**

*Berkeley Seismological Laboratory and Department of Earth and Planetary Science, Berkeley, California 94720, USA*

**For decades there has been a vigorous debate about the depth extent of continental roots[1,2]. The analysis of heat-flow[3], mantle-xenolith[4] and electrical-conductivity[5] data all indicate that the coherent, conductive part of continental roots (the 'tectosphere') is at most 200–250 km thick. Some global seismic tomographic models agree with this estimate, but others suggest that a much thicker zone of high velocities lies beneath continental shields[6–9], reaching a depth of at least 400 km. Here we show that this disagreement can be reconciled by taking into account seismic anisotropy. We show that significant radial anisotropy, with horizontally polarized shear waves travelling faster than those that are vertically polarized, is present under most cratons in the depth range 250–400 km—similar to that found under ocean basins[9,10] at shallower depths of 80–250 km. We propose that, in both cases, the anisotropy is related to shear in a low-viscosity asthenospheric channel, located at different depths under continents and oceans. The seismically defined 'tectosphere' is then at most 200–250 km thick under old continents. The 'Lehmann discontinuity', observed mostly under continents at about 200–250 km, and the 'Gutenberg discontinuity', observed under oceans at depths of about 60–80 km, may both be associated with the bottom of the lithosphere, marking a transition to flow-induced asthenospheric anisotropy.**

The maximum thickness of the lithosphere, defined as a region of distinctly faster than average seismic velocities (1.5%–2%) in global S-wave velocity $V_S$ tomographic models, ranges from 200 to 400 km, depending on the model[6–9]. This is clear from the drop in correlation between some models from around 0.80 at 100 km to less than 0.45 at 300 km depth (Fig. 1a), which casts some doubt on the ability of global tomography to accurately resolve upper mantle structure. However, although global $V_S$ models differ from each other significantly in the depth range 200–400 km under the main continental shields, these differences are consistent when they are classified into three categories, depending on the type of data used to derive them: 'SV' (mostly vertical or longitudinal component data, dominated by Rayleigh waves in the upper mantle), 'SH' (mostly transverse component data, dominated by Love waves), and 'hybrid' (three-component data). SH and hybrid models are better

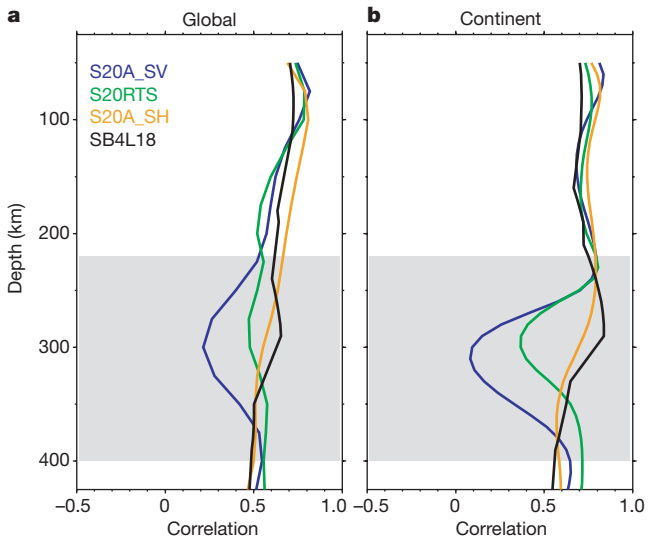


**Figure 1** Correlation coefficient as a function of depth between model SAW24B16[8], an SH model, and other global tomographic S velocity models. **a**, Correlation computed over the whole globe; **b**, correlation computed over continental areas only. Here continents include all areas of elevation greater than −0.5 km. Note that models S20A_SH[9] (an SH model) and SB4L18[6] (a hybrid model) correlate better with SAW24B16 than models S20A_SV[9] and S20RTS[7], which are both SV models. The reduced correlation in the depth range 250–400 km between SH/hybrid models and SV models is strongly accentuated over continents.

correlated with each other than with SV models. This difference is accentuated when the correlation is computed only across continental areas (Fig. 1b). Also, SH (and hybrid) models exhibit continental roots that exceed those of SV models by 100 km or more, as illustrated in Fig. 2 (see also Supplementary Fig. 1).

On the other hand, global tomographic studies that account for seismic anisotropy, either by inverting separately for $V_{SV}$ and $V_{SH}$[9], or in the framework of more general anisotropic theory[10], have documented significant lateral variations in the anisotropic parameter $\xi = (V_{SH}/V_{SV})^2$ on the global scale. Until now, attention has mostly focused on the strong positive $\delta \ln \xi$ ($\delta \ln V_{SH} > \delta \ln V_{SV}$) observed in the central part of the Pacific Ocean in the depth range 80–200 km. The presence of this anisotropy has been related to shear flow in the asthenosphere, with a significant horizontal component. Deeper anisotropy was suggested, but not well resolved in these studies, either because the data set was limited to fundamental mode surface waves[10], or because of the use of inaccurate depth sensitivity kernels[9]. In particular, it is important to verify that any differences in $V_{SV}$ and $V_{SH}$ observed below a depth of 200 km are not an artefact of simplified theoretical assumptions, which ignore the influence of radial anisotropy on depth sensitivity kernels (see Supplementary Fig. 2 for a comparison of isotropic and anisotropic $V_S$ kernels).

We have developed an inversion procedure for transverse isotropy using three-component surface and body waveform data, in the framework of normal mode asymptotic coupling theory[11], which in particular, involves the use of two-dimensional broadband anisotropic sensitivity kernels appropriate for higher modes and body waves (see Methods section). Figure 3 shows the distributions of $\delta \ln \xi$ in the resulting degree-16 anisotropic model (SAW16AN) (for the corresponding distributions in $V_{SH}$, $V_{SV}$, see Supplementary Fig. 3), at depths of 175 km, 300 km and 400 km. At 175 km depth, the global distribution of $\delta \ln \xi$ confirms features found in previous studies, and is dominated by the striking positive $\delta \ln \xi$ ($V_{SH} > V_{SV}$) anomaly in the central Pacific[9,10] and a similar one in the Indian Ocean. However, at depths greater than 250 km, the character of the distribution changes: positive $\delta \ln \xi$ emerges under the Canadian Shield, Siberian Platform, Baltic Shield, southern Africa, Amazonian and Australian cratons, while the positive $\delta \ln \xi$ fades out under the Pacific and Indian oceans. At 300 km depth, the roots of most cratons are characterized by positive $\delta \ln \xi$, which extend down to about 400 km. These features are emphasized in depth cross-sections across major continental shields (Fig. 4), where we compare $V_{SH}$ and $V_{SV}$ distributions, consistently showing deeper continental roots in $V_{SH}$. The presence of anisotropy at depths over 200 km, with $V_{SH} > V_{SV}$, is also consistent with some

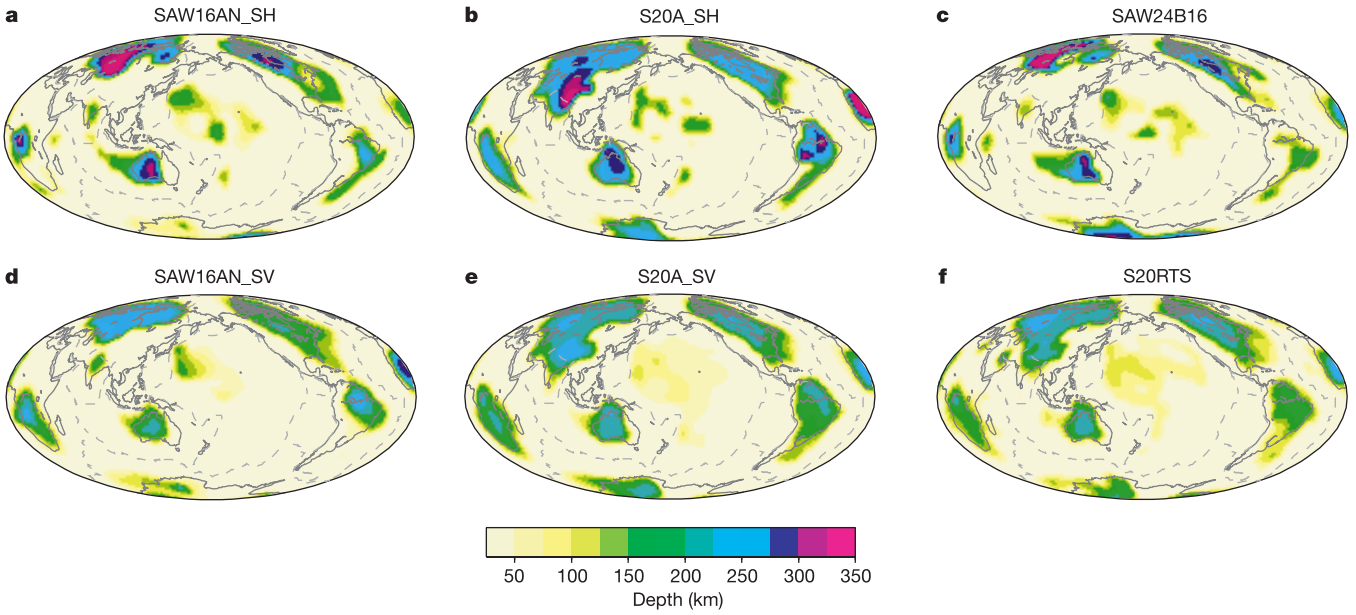


**Figure 2** Maximum depth for which the velocity anomaly with respect to the reference model PREM[28] is greater than 2%, for different S velocity models. **a**–**c**, SH-type models; **d**–**e**, SV-type models. **c**, **f**, $V_{SH}$ model SAW24B16[8] compared to $V_{SV}$ model S20RTS[7]. **b**, **e**, SH and SV parts of model S20A[9], obtained by inverting T-component data and Z,L-component data separately. **a**, **d**, SH and SV parts of anisotropic model SAW16AN discussed here. While the roots of continents generally extend to depths greater than 300–350 km in SH models, they do not exceed 200–250 km in SV models.

regional studies[12,13]. Interestingly, the East Pacific Rise has a signature with $\delta \ln \xi < 0$ down to 300 km, indicative of a significant component of vertical flow. At 400 km depth, we also note the negative $\delta \ln \xi$ around the Pacific ring, consistent with quasi-vertical flow in the subduction zone regions in the western Pacific and South America.

There has been a long-lasting controversy regarding the interpretation of shear wave splitting observations under continents, with some authors advocating frozen anisotropy in the lithosphere[14], and others, flow-induced anisotropy related to present-day plate motions[15]. SKS splitting measurements do not have adequate depth resolution, and inferences that have been made on the basis of a lithospheric thickness of 400 km or more under cratons need to be revisited.

Temperatures in the 250–400 km depth range exceed 1,000 °C, and are therefore too high to allow sustained frozen anisotropy in a mechanically coherent lithospheric lid on geologically relevant timescales[15]. Therefore we infer that the $V_{SH} > V_{SV}$ anisotropy we describe here must be related to present-day flow-induced shear, with a significant horizontal component. Such an interpretation is also compatible with results from shear wave splitting, which document the presence of anisotropy below cratons indicating simple-shear deformation parallel to present-day plate motion, at least in North America[16,17] and Australia[13]: some recent studies indicate that there may be two zones of SKS anisotropy under continental shields, one shallower, reflecting past geological events, and one deeper, related to present-day flow[16,18].

We note the similarity of the character of $V_{SH} > V_{SV}$ anisotropy, in the depth range 200–400 km under cratons, and 80–200 km under ocean basins, and we suggest that both are related to shear in the asthenosphere, the difference in depth simply reflecting the varying depth of the asthenospheric channel. Although our inference is indirect, it reconciles tomographic studies with other geophysical observations of lithospheric thickness based on heat flow[3], xenoliths[4] and mantle electrical conductivity[5]. It is also in agreement with lateral variations in attenuation on the global scale[19].

Another contentious issue is the nature of the Lehmann discontinuity, and in particular the puzzling observation that it is not a consistent global feature[20], but is observed primarily in stable continental areas and not under oceans[21,22]. Leven *et al.*[23] first proposed that the Lehmann might be a discontinuity in anisotropic structure, and more recent studies have suggested that it is a rheological boundary marking a transition from anisotropic to isotropic structure[24–25]. Because the $V_{SH} > V_{SV}$ anisotropy under continental cratons is found deeper than 200 km, we propose that the Lehmann discontinuity actually marks the top of the asthenospheric layer, a transition from weak anisotropic lowermost continental lithosphere to anisotropic asthenosphere, in agreement with the inference of ref. 23. Under oceans, the lithosphere is much thinner, and the lithosphere/asthenosphere boundary occurs at much shallower depths. There is no consistently observed discontinuity around 200–250 km depth[20]. On the other hand, the shallower Gutenberg discontinuity is often reported under oceans

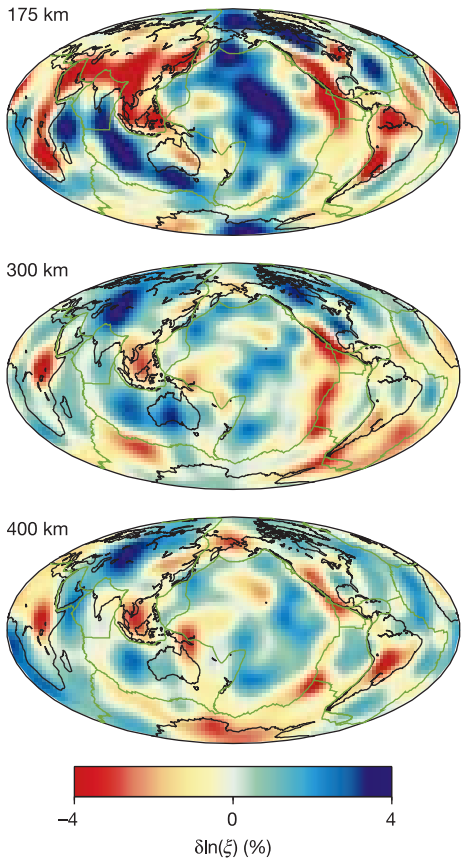


**Figure 3** Maps of relative lateral variations in the anisotropic parameter $\delta \ln \xi$ of model SAW16AN at three depths in the upper mantle. $\delta \ln \xi > 0$ in regions where $V_{SH} > V_{SV}$ and $\delta \ln \xi < 0$ in regions where $V_{SV} < V_{SH}$. Lateral variations are referred to reference model PREM[28], which is isotropic below 220 km depth, but has significant $\delta \ln \xi > 0$ at 175 km depth. Note how the regions of strong positive $\delta \ln \xi$ shift from the central Pacific to continental areas between 175 and 300 km depth. At depths shallower than 200 km, continental shields have mostly $\delta \ln \xi < 0$, as noted previously[29]. At 300 km depth, continental shields are no longer prominent in $V_{SV}$. At depths greater than 350 km, the subduction zones are more prominent in $V_{SV}$ than in $V_{SH}$, resulting in $\delta \ln \xi < 0$ around the Pacific, indicative of vertical flow. The East Pacific Rise appears as a zone of vertical flow to depths in excess of 300 km. Depth resolution is of the order of ±50 km.

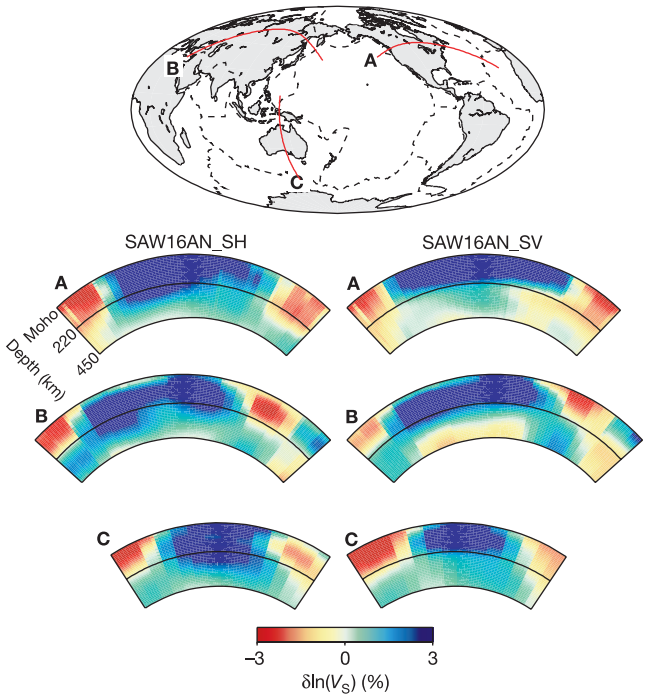


**Figure 4** Depth cross-sections through three continents (see locations at top) showing the SH (left) and SV (right) components of anisotropic model SAW16AN. The SH sections consistently indicate fast velocities extending to depths in excess of 220 km, whereas the SV sections do not. In section B, the higher velocity associated with the subduction under the area north of Japan is clearly visible in SV but not so much in SH. This anisotropy may contribute to explaining why subduction zones are generally less visible in S tomographic models (mostly of the hybrid type, which thus more sensitive to SH) than in P models.

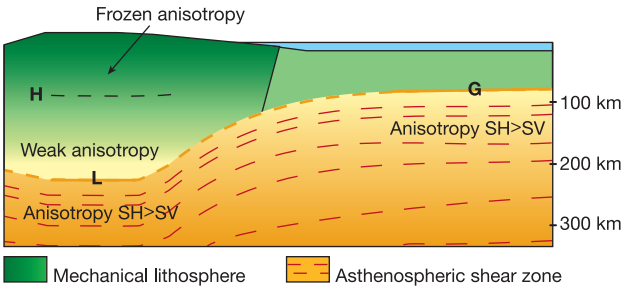


**Figure 5** Sketch illustrating our interpretation of the observed anisotropy in relation to lithospheric thickness, and its relationship to the Lehmann (L) and Gutenberg (G) discontinuities. The Hales discontinuity (H), which is also shown, is generally observed as a positive impedance embedded within the continental lithosphere in the depth range 60–80 km (ref. 30). H and G may not be related.

and appears as a negative impedance reflector in studies of precursors to multiple ScS reverberations[22]. The difference in depth of the observed $\delta \ln \xi > 0$ anisotropy between continents and oceans is consistent with an interpretation of both the Lehmann and Gutenberg discontinuities as marking the bottom of the mechanically coherent lithosphere, in areas where it is quasi-horizontal (Fig. 5).

In this study, we consider only radial anisotropy, which in particular does not account for intermediate orientation of the fast axis of anisotropy[10]. We can only infer that regions with significant $\delta \ln \xi > 0$ are regions where anisotropy has a significant horizontal component, and expresses the alignment of olivine crystals in predominantly horizontal flow[26]. In regions of transition between cratons and younger continental provinces, or between ocean and continent, the asthenospheric flow would follow the inclined shape of the bottom of the lithosphere and be less clearly detected with our approach.

Thus, the inspection of radial anisotropy in the depth range 200–400 km allows us to infer that continental roots do not extend much beyond a depth of 250 km, in agreement with other geophysical observations. The part of the mantle under old continents that translates coherently with plate motions need not be thicker than 200–250 km. Tomographic models reveal the varying depth of the top of the anisotropic asthenospheric channel, marked by the Lehmann discontinuity under continents (about 200–250 km depth), and the Gutenberg discontinuity under oceans (about 60–80 km depth). Seemingly incompatible tomographic models obtained by different researchers can thus also be reconciled: the relatively poor correlation between different models in the depth range 250–400 km is not due to a lack of resolution of the tomographic approach, but rather to the different sensitivity to anisotropy of different types of data. □

## Methods

### Broadband sensitivity kernels

In this study, we invert three-component long-period seismograms in the time domain (down to periods of 60 s for surface waves, and 32 s for body waves) in the framework of nonlinear asymptotic coupling theory (NACT[11]), a normal-mode perturbation-based approach which takes into account the concentrated sensitivity of body waves to structure along the ray path, in contrast to standard approaches which assume one-dimensional kernels, an approximation which is valid only for fundamental mode surface waves. Our technique involves dividing the seismogram into wavepackets that may contain one or more seismic phases, and applying weighting factors to equalize the contribution of large and small amplitude wavepackets in the least-squares inversion.

### Transverse isotropy

A transversely isotropic medium with vertical axis of symmetry is described by density $\rho$ and five elastic parameters, usually $A = \rho V_{PH}^2$, $C = \rho V_{PV}^2$, $L = \rho V_{SV}^2$, $N = \rho V_{SH}^2$ and $F$. We start by considering, equivalently, the six parameters $V_{SH}$, $V_{SV}$, $\eta = F/(A - 2L)$, $V_{P_{iso}}$ (isotropic $V_P$), $\phi = C/A$ and $\rho$, with appropriate kernels for weak transverse anisotropy. To reduce the number of parameters in the inversion and keep only those that are best-resolved ($V_{SH} = (N/\rho)^{1/2}$, $V_{SV} = (L/\rho)^{1/2}$), we assume the following scaling relations, as inferred from laboratory experiments for depths relevant to our study (that is, less than 500 km)[27]: $\delta \ln V_{P_{iso}} = 0.5\delta \ln V_{S_{iso}}$, $\delta \ln \eta = -2.5\delta \ln \xi$ and $\delta \ln \phi = -1.5\delta \ln \xi$, with $\delta \ln V_{S_{iso}} = 2/3\delta \ln V_{SV} + 1/3\delta \ln V_{SH}$ (under the assumption of weak anisotropy; $V_{S_{iso}}$ is isotropic $V_S$ and $\delta \ln \rho = 0.3\delta \ln V_{S_{iso}}$. We have verified that the main features in our results are not affected by the particular values chosen in these relations. Starting from our most recent tomographic models, SAW24B16[8] for $V_{SH}$ and SAW16BV[19] for $V_{SV}$, we invert for perturbations in $V_{SH}$ and $V_{SV}$ in a spherical harmonics expansion up to degree 16 laterally. Vertical parametrization is in terms of cubic splines. Since our sampling of the lowermost mantle with SV-sensitive body waves is limited, in order to avoid bias from anisotropy in D″, we have restricted our inversion to the top 1,500 km of the mantle, and chosen the body waveforms to include in the data set accordingly.

We have checked that our results, and in particular the observation of radial anisotropy under continents at depths greater than 200 km is not the result of artefacts due to poor resolution in the inversion for either $V_{SH}$ or $V_{SV}$, by performing synthetic tests. For example, Supplementary Fig. 4 shows the results of an experiment in which synthetic transverse component seismograms have been computed for a starting SV model (no roots below 250 km), mimicking the actual distribution of our data set, and then reinverted for an SH model. No deep continental roots are apparent in the resulting final model.

Assuming lattice preferred orientation of anisotropic minerals such as olivine, and as illustrated, for example, in ref. 26, a large-scale predominantly horizontal flow is characterized by a positive $\delta \ln \xi$ and also by significant SKS wave splitting. The direction of the fast axis inferred from the latter is related to the direction of the flow in the horizontal plane. Coupling between Love and Rayleigh waves that may arise in the case of anisotropy with a non-vertical axis of symmetry affects mainly the wave amplitudes. Because we are primarily fitting the phase part of the seismograms, such coupling should have little effect on our results.

Received 18 September 2002; accepted 4 March 2003; doi:10.1038/nature01559.


1. Jordan, T. H. The continental lithosphere. *Rev. Geophys. Space Phys.* **13,** 1–12 (1975).
2. Anderson, D. L. The deep structure of continents. *J. Geophys. Res.* **84,** 7555–7560 (1990).
3. Jaupart, C., Mareschal, J. C. & Guillou-Frottier, L. Heat flow and thickness of the lithosphere in the Canadian Shield. *J. Geophys. Res.* **103,** 15269–15286 (1998).
4. Rudnick, R., McDonough, W. & O'Connell, R. Thermal structure, thickness and composition of continental lithosphere. *Chem. Geol.* **145,** 395–411 (1998).
5. Hirth, G., Evans, R. L. & Chave, A. D. Comparison of continental and oceanic mantle electrical conductivity: Is the Archean lithosphere dry? *Geochem. Geophys. Geosyst.* **1,** 2000GC000048 (2000).
6. Masters, G., Johnson, S., Laske, G. & Bolton, B. A shear-velocity model of the mantle. *Phil. Trans. R. Soc. Lond. A* **354,** 1385–1411 (1996).
7. Ritsema, J., van Heijst, H. & Woodhouse, J. H. Complex shear wave velocity structure imaged beneath Africa and Iceland. *Science* **286,** 1925–1928 (1999).
8. Mégnin, C. & Romanowicz, B. The 3D shear velocity structure of the mantle from the inversion of body, surface and higher mode waveforms. *Geophys. J. Int.* **143,** 709–728 (2000).
9. Ekström, G. & Dziewonski, A. M. The unique anisotropy of the Pacific upper mantle. *Nature* **394,** 168–172 (1998).
10. Montagner, J. P. What can seismology tell us about mantle convection? *Rev. Geophys.* **32**(2), 135–137 (1994).
11. Li, X. D. & Romanowicz, B. Comparison of global waveform inversions with and without considering cross branch coupling. *Geophys. J. Int.* **121,** 695–709 (1995).
12. Tong, C., Gudmundsson, O. & Kennett, B. L. N. Shear wave splitting in refracted waves returned from the upper mantle transition zone beneath northern Australia. *J. Geophys. Res.* **99,** 15783–15797 (1994).
13. Debayle, E. & Kennett, B. L. N. Anisotropy in the Australasian upper mantle from Love and Rayleigh waveform inversion. *Earth Planet. Sci. Lett.* **184,** 339–351 (2000).
14. Silver, P. G. Seismic anisotropy beneath the continents: probing the depths of geology. *Annu. Rev. Earth Planet. Sci.* **24,** 385–432 (1996).
15. Vinnik, L. P., Makeyeva, L. I., Milev, A. & Usenko, Y. Global patterns of azimuthal anisotropy and deformations in the continental mantle. *Geophys. J. Int.* **111,** 433–447 (1992).
16. Fouch, M. J., Fischer, K. M., Parmentier, E. M., Wysession, M. E. & Clarke, T. J. Shear wave splitting, continental keels, and patterns of mantle flow. *J. Geophys. Res.* **105,** 6255–6275 (2000).
17. Bokelmann, G. H. R. Which forces drive North America? *Geology* **30**(11), 1027–1030 (2002).
18. Levin, V., Menke, W. & Park, J. Shear wave splitting in the Appalachians and the Urals: a case for multilayered anisotropy. *J. Geophys. Res.* **104,** 17975–17993 (1999).
19. Romanowicz, B. & Gung, Y. Superplumes from the core-mantle boundary to the lithosphere: implications for heat flux. *Science* **296,** 513–516 (2002).
20. Shearer, P. Seismic imaging of upper mantle structure with new evidence for a 520 km discontinuity. *Nature* **344,** 121–126 (1990).
21. Gu, Y. M., Dziewonski, A. M. & Ekström, G. Preferential detection of the Lehmann discontinuity beneath continents. *Geophys. Res. Lett.* **28,** 4655–4658 (2001).
22. Revenaugh, J. & Jordan, T. H. Mantle layering from ScS reverberations. 3. The upper mantle. *J. Geophys. Res.* **96,** 19781–19810 (1991).
23. Leven, J. H., Jackson, I. & Ringwood, A. E. Upper mantle seismic anisotropy and lithospheric decoupling. *Nature* **289,** 234–239 (1981).
24. Karato, S. I. On the Lehmann discontinuity. *Geophys. Res. Lett.* **19,** 2255–2258 (1992).
25. Gaherty, J. B. & Jordan, T. H. Lehmann discontinuity as the base of an anisotropic layer beneath continents. *Science* **268,** 1468–1471 (1995).
26. Montagner, J.-P. Upper mantle low anisotropy channels below the Pacific Plate. *Earth Planet. Sci. Lett.* **202,** 263–274 (2002).
27. Montagner, J. P. & Anderson, D. L. Petrological constraints on seismic anosotropy. *Phys. Earth Planet. Int.* **54,** 82–105 (1989).
28. Dziewonski, A. M. & Anderson, D. L. Preliminary reference earth model. *Phys. Earth Planet. Int.* **25,** 297–356 (1981).
29. Babuska, V., Montagner, J. P., Plomerova, J. & Girardin, N. Age-dependent large-scale fabric of the mantle lithosphere as derived from surface wave velocity anisotropy. *Pure Appl. Geophys.* **121,** 257–280 (1998).

30. Levin, V. & Park, J. Shear zones in the Proterozoic lithosphere of the Arabian Shield and the nature of the Hales discontinuity. *Tectonophysics* **323**(3–4), 131–148 (2000).

**Supplementary Information** accompanies the paper on *Nature*'s website (**http://www.nature.com/nature**).

**Acknowledgements** We thank J. Park, B. Kennett and J. P. Montagner for constructive comments on this manuscript. This work was supported through a grant from the National Science Foundation.

**Competing interests statement** The authors declare that they have no competing financial interests.

**Correspondence** and requests for materials should be addressed to B.R. (e-mail: barbara@seismo.berkeley.edu).

# Soil invertebrate fauna enhances grassland succession and diversity

**Gerlinde B. De Deyn*, Ciska E. Raaijmakers*, H. Rik Zoomer†, Matty P. Berg†, Peter C. de Ruiter‡, Herman A. Verhoef†, T. Martijn Bezemer* & Wim H. van der Putten***

* *Department of Multitrophic Interactions, Centre for Terrestrial Ecology, Netherlands Institute of Ecology (NIOO-KNAW), P.O. Box 40, 6666 ZG, Heteren, The Netherlands*
† *Department of Animal Ecology, Institute of Ecological Science, Vrije Universiteit De Boelelaan 1085, 1081 HV Amsterdam, The Netherlands*
‡ *Department of Environmental Sciences, Copernicus Research Institute for Sustainable Development and Innovation, Utrecht University, P.O. Box 80115, 3508 TC Utrecht, The Netherlands*

**One of the most important areas in ecology is to elucidate the factors that drive succession in ecosystems and thus influence the diversity of species in natural vegetation. Significant mechanisms in this process are known to be resource limitation[1–3] and the effects of aboveground vertebrate herbivores[4,5]. More recently, symbiotic and pathogenic soil microbes have been shown to exert a profound effect on the composition of vegetation[6–9] and changes therein[10,11]. However, the influence of invertebrate soil fauna on succession has so far received little attention[12,13]. Here we report that invertebrate soil fauna might enhance both secondary succession and local plant species diversity. Soil fauna from a series of secondary grassland succession stages selectively suppress early successional dominant[14] plant species, thereby enhancing the relative abundance of subordinate[14] species and also that of species from later succession stages. Soil fauna from the mid-succession stage had the strongest effect. Our results clearly show that soil fauna strongly affects the composition of natural vegetation and we suggest that this knowledge might improve the restoration and conservation of plant species diversity.**

The succession of species in natural communities is one of the most fundamental concepts in ecology[15]. Successional patterns in vegetation can be reasonably well predicted owing to their correlation with changes in resource availability, whereas the competitive abilities of plants for these resources determines which species might become dominant[2]. However, biotic interactions above and below ground can greatly change the outcome of these competitive interactions. Aboveground vertebrate herbivores can indirectly benefit subdominant plant species through selective feeding on dominants[4,5]. Below the soil surface, root symbionts can enhance plant species diversity by improving the nutrient uptake and growth of subdominants[6], and root pathogens can do so by suppressing dominant host plant species[7]. Selective improvement or suppression of plant species can eventually lead to cyclic[8,9,16] or unidirectional successional[11] shifts in local species composition.

Although soil microorganisms seem to have a profound effect on vegetation succession and plant species diversity, the role of invertebrate soil fauna has not yet been resolved. In early secondary succession grasslands, the application of soil insecticides reduces the abundance of root-feeding insects, resulting in the promotion of early successional forbs[12], suggesting that root-feeding insects might enhance the process of succession[13]. Similar effects of root-feeding insects were confirmed in microcosm[17] and mesocosm[18] studies. In mid-succession extensively grazed grasslands, cyclic replacement of grass and sedge species were correlated primarily with the abundance of plant-feeding nematodes[19]. However, soil organisms with a larger body size seem to overrule the effects of smaller soil organisms[18], casting doubt on the results of studies that focus on the role of specific components of invertebrate soil fauna.

To clarify the specific contribution of the invertebrate soil fauna (hereafter called 'soil fauna') to secondary vegetation succession and to plant species diversity, we conducted an experiment in which natural soil fauna communities (Table 1) were applied to combinations of plant species from production, restoration and conservation grasslands. We constructed experimental grassland communities in which plant species from a production grassland (early succession stage), from a grassland subjected to nature restoration management during the past 20 years (mid-succession) and from a species-rich natural grassland community (the target of secondary grassland succession) were grown in mixed stands. All plant communities were established in sterilized soil and were inoculated with soil fauna from one of the three successional stages. This made it possible to determine the role of the soil fauna from a range of secondary succession grasslands on the outcome of interactions between the plant species from their own and from the other two successional stages. The soil fauna added represented the densities and composition of the field communities and included microfauna (nematodes), mesofauna (micro-arthropods) and macrofauna (beetle larvae).

Our results show that the addition of all three successional communities of soil fauna resulted in significant shifts in the

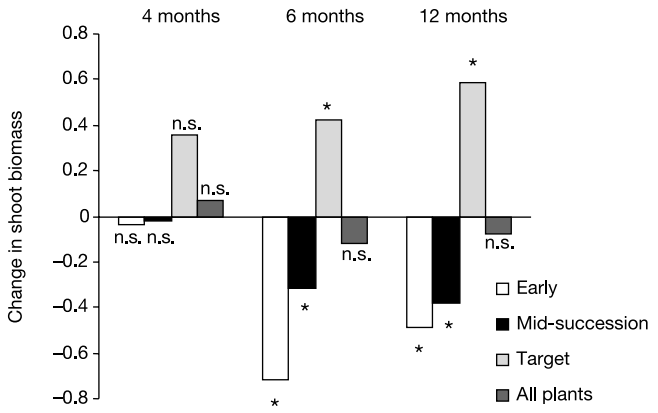


**Figure 1** Change in the shoot biomass of early and mid-succession plant species and plants from the target grassland community in the presence of soil fauna relative to the control (no soil fauna added) calculated as $(B_i - B_c)/B_c$, where $B_i$ and $B_c$ are the mean shoot biomasses with and without soil fauna added, respectively. The experimental grassland communities were grown in microcosms for 1 year. Addition of the soil fauna impaired the early and mid-succession plants and stimulated the development of plants from the target grassland community. Data presented are averages over all treatments with different origins of soil fauna. Significance: asterisk, $P < 0.05$; n.s., not significant.